

Ultrafast antiferromagnet rearrangement in Co/IrMn/CoGd trilayers

Zongxia Guo(郭宗夏), Gregory Malinowski, Pierre Vallobra, Yi Peng(彭懿), Yong Xu(许涌), Stéphane Mangin, Weisheng Zhao(赵巍胜), Michel Hehn, and Boyu Zhang(张博宇)

Citation: Chin. Phys. B, 2023, 32 (**8**): 087507. DOI: 10.1088/1674-1056/acda83

Journal homepage: http://cpb.iphy.ac.cn; http://iopscience.iop.org/cpb

What follows is a list of articles you may be interested in

Magnetic and electronic properties of bulk and two-dimensional $FeBi_2Te_4$: A first-principles study

Qianqian Wang(王倩倩), Jianzhou Zhao(赵建洲), Weikang Wu(吴维康), Yinning Zhou(周胤宁), Qile Li, Mark T. Edmonds, and Shengyuan A. Yang(杨声远)

Chin. Phys. B, 2023, 32 (**8**): 087506. DOI: 10.1088/1674-1056/acd522

Low-temperature ferromagnetism in tensile-strained $LaCoO_{2.5}$ thin film

Yang-Yang Fan(范洋洋), Jing Wang(王晶), Feng-Xia Hu(胡凤霞), Bao-He Li(李宝河), Ai-Cong Geng(耿爱丛), Zhuo Yin(殷卓), Cheng Zhang(张丞), Hou-Bo Zhou(周厚博), Meng-Qin Wang(王梦琴), Zi-Bing Yu(尉紫冰), and Bao-Gen Shen(沈保根)

Chin. Phys. B, 2023, 32 (**8**): 087504. DOI: 10.1088/1674-1056/acafdc

Out-of-plane weak ferromagnetism at room temperature in lattice-distortion non-collinear antiferromagnet of single-crystal Mn_3Sn

Bo-Xi Zhang(张博熙), Ping Song(宋平), Shan-Shan Deng(邓珊珊), Li Lou(娄理), and Sen Yao(姚森)

Chin. Phys. B, 2023, 32 (**8**): 087502. DOI: 10.1088/1674-1056/acca0b

Magnetic ordering induced magnetodielectric effect in $Ho_2Cu_2O_5$ and $Yb_2Cu_2O_5$

Hao Jin(金昊), Shuai Huang(黄帅), Kai-Qi Wan(万凯奇), Chang-Ming Zhu(朱长明),Hai-Ou Wang(王海欧), Kun-Peng Su(苏昆朋), and De-Xuan Huo(霍德璇)

Chin. Phys. B, 2023, 32 (**6**): 067504. DOI: 10.1088/1674-1056/ac904a

Crystal growth of $CeMn_{0.85}Sb_2$: Absence of magnetic order of Ce-sublattice

Yong Li(李勇), Shan-Shan Miao(苗杉杉), Hai Feng(冯海),Huai-Xin Yang(杨槐馨), and You-Guo Shi(石友国)

Chin. Phys. B, 2023, 32 (**6**): 067501. DOI: 10.1088/1674-1056/acc060

RAPID COMMUNICATION

Ultrafast antiferromagnet rearrangement in Co/IrMn/CoGd trilayers

Zongxia Guo(郭宗夏)[1,2], Gregory Malinowski[2], Pierre Vallobra[1,3], Yi Peng(彭懿)[2], Yong Xu(许涌)[1,3], Stéphane Mangin[2], Weisheng Zhao(赵巍胜)[1,3], Michel Hehn[2], and Boyu Zhang(张博宇)[1,†]

[1] *Fert Beijing Institute, School of Integrated Science and Engineering, Beihang University, Beijing* 100191, *China*
[2] *Université de Lorraine, CNRS, IJL, Nancy,* 54011 *France*
[3] *Hefei Innovation Research Institute, Beihang University, Hefei* 230012, *China*

(Received 23 March 2023; revised manuscript received 29 May 2023; accepted manuscript online 1 June 2023)

Antiferromagnets offer great potential for high-speed data processing applications, as they can expend spintronic devices from a static storage and gigahertz frequency range to the terahertz range. However, their zero net magnetization makes them difficult to manipulate and detect. In recent years, there has been a lot of attention given to the ultrafast manipulation of magnetic order using ultra-short single laser pulses, but it remains unknown whether a similar scenario can be observed in antiferromagnets. In this work, we demonstrate the manipulation of antiferromagnets with a single femtosecond laser pulse in perpendicular exchange-biased Co/IrMn/CoGd trilayers. We study the dual exchange bias interlayer interaction in quasi-static conditions and competition in ultrafast antiferromagnet rearrangement. Our results show that, compared to conventional ferromagnetic/antiferromagnetic systems, the IrMn antiferromagnet can be ultrafast and efficiently manipulated by the coupled CoGd ferrimagnetic layer, which paves the way for potential energy-efficient spintronic devices.

Keywords: antiferromagnet, ferrimagnet, exchange bias, all-optical switching

PACS: 75.47.–m, 85.75.–d, 71.70.Ej **DOI:** 10.1088/1674-1056/acda83

1. Introduction

Antiferromagnets with anti-aligned spin sublattices, which have zero dipolar fields, possess advantageous properties such as insensitivity to interfering magnetic fields, enhanced stability, and ultrafast spin dynamics that may find applications in a broad range from data processing to magnetic memory.[1,2] However, the lack of a net magnetic moment poses a challenge for manipulation and detection.[2] This is usually achieved using the exchange bias effect (shift of the hysteresis loop along the magnetic field direction), where the antiferromagnet (AFM) controls the orientation of a coupled ferromagnet (FM), which can then be controlled and detected using conventional method.[3,4] The exchange bias field (H_e) depends strongly on the layers thicknesses, texture, and the magnetic configuration in both FM and AFM layers.[5,8] The exchange bias phenomenon is usually considered as an interfacial effect, but recent studies also indicated that the AFM volume also plays a role in defining the exchange bias.[9–12]

The wide applications of spintronic sensors[13] and magnetic random-access memories (MRAM)[14] have extended the capabilities of exchange bias systems. However, the conventional method of setting the exchange bias field typically takes several hours and involves annealing with or without a field.[4,15] Recently, femtosecond-laser-induced all-optical switching has been attracting much attention.[16–18] The field-free switching of [Co/Pt] multilayers can be realized by using all-optical helicity-dependent switching (AO-HDS) with multi-pulses, which allows for the reversal of the perpendicular exchange bias in $[Co/Pt]_n$/IrMn multilayers.[19] Additionally, Gd-based ferrimagnets (FiM) alloys have been found to show all-optical helicity-independent switching (AO-HIS) with a single femtosecond laser excitation,[20] allowing for exchange bias switching to be compressed within a hundred picoseconds.[21] The exchange bias reversal in such a short time scale also indicates the ultrafast rearrangement of the AFM order. Due to the difficulties in the direct characterization of interfacial and volume AFM spin structures in the thin film structure, most of the studies rely on the dual exchange bias trilayer structures consisting of an FM/AFM/FM stack,[9–11] where the dual exchange bias behavior is used to explore the AFM volume order configuration. These studies are all based on long timescale field-cooling configurations,[9] but the ultrafast rearrangement of AFM orders and exchange bias have not yet been systematically investigated experimentally.

In this paper, we demonstrate the manipulation of exchange bias in Co/IrMn/CoGd (FM/AFM/FiM) trilayers with dual perpendicular exchange bias using a single femtosecond laser pulse. In quasi-static characteristics, we show the IrMn thickness-dependent interlayer interaction of the dual exchange bias interface. With the single femtosecond laser excitation, we find that the exchange bias switching is generated from the ultrafast rearrangement of the AFM spins at the IrMn/CoGd interface and further demonstrate the competition across the AFM volume orders. In addition, the high

†Corresponding author. E-mail: boyu.zhang@buaa.edu.cn
© 2023 Chinese Physical Society and IOP Publishing Ltd

repeatable exchange bias switching of IrMn/CoGd presents an ultrafast and efficient method for manipulation, offering novel insights into the potential applications of spintronic devices in the future.

2. Stacks structure and interplay of the dual exchange bias interfaces

All the samples were deposited onto glass substrates by magnetron sputtering. The trilayer systems of the glass/Ta (5)/Pt (5)/Co (1)/$Ir_{20}Mn_{80}(t_{IrMn})$/$Co_{77}Gd_{23}$ (4)/Pt (5) (thicknesses in nm) with t_{IrMn} = 2–8 nm are shown in Fig. 1(a). In the CoGd amorphous layer, the magnetization of the Gd sublattice is antiferromagnetically exchanged coupled to the magnetization of the Co sublattice. The net magnetization of the alloy is given by the contribution of both sublattices and reaches zero (the compensation concentration) at room temperature for a composition between 30% and 32%. Here, we focus on Co-rich alloy with a 23% Gd concentration. After deposition, the samples were annealed for 1 h at 200 °C in an out-of-plane magnetic field of −60 mT. The perpendicular magnetic anisotropy and exchange bias of the trilayers were confirmed by the polar magneto-optic Kerr effect (MOKE). A series of stepped hysteresis loops are obtained in Fig. 1(b). The exchange bias field $\mu_0 H_e$ and coercivity $\mu_0 H_c$ of both interfaces as a function of the IrMn thickness are presented in Fig. 1(c). A noticeable exchange bias field of both interfaces can be observed over the 2 nm IrMn, reaching the maximum at t_{IrMn} = 5 nm and decreasing when t_{IrMn} is further increased. The coercivity $\mu_0 H_c$ decreases with increasing t_{IrMn}. According to Meiklejohn's macrospin model,[3] the effective exchange coupling constant in an FM/AFM bilayer is evaluated using $J_{ex} = \mu_0 H_e M_s t$, where M_s is the saturation magnetization of the CoGd (or Co) layer, which is obtained by SQUID-VSM, and t is the CoGd (or Co) layer thickness. We observe that the nearly compensated CoGd layer exhibits a larger exchange bias field than the Co/IrMn interface at t_{IrMn} between 3 nm and 8 nm, as illustrated in Fig. 1(c). The observed distinction can be ascribed to the different magnetic disorder conditions present at the top and bottom interfaces during deposition.[20] These conditions induce stronger exchange interactions at the IrMn/CoGd interface when t_{IrMn} is between 3 nm and 6.5 nm, as shown in Fig. 1(d). Additionally, the near compensated CoGd alloy, characterized by a low M_s, also demonstrates a greater exchange bias field for a comparable J_{ex} at t_{IrMn} = 8 nm.

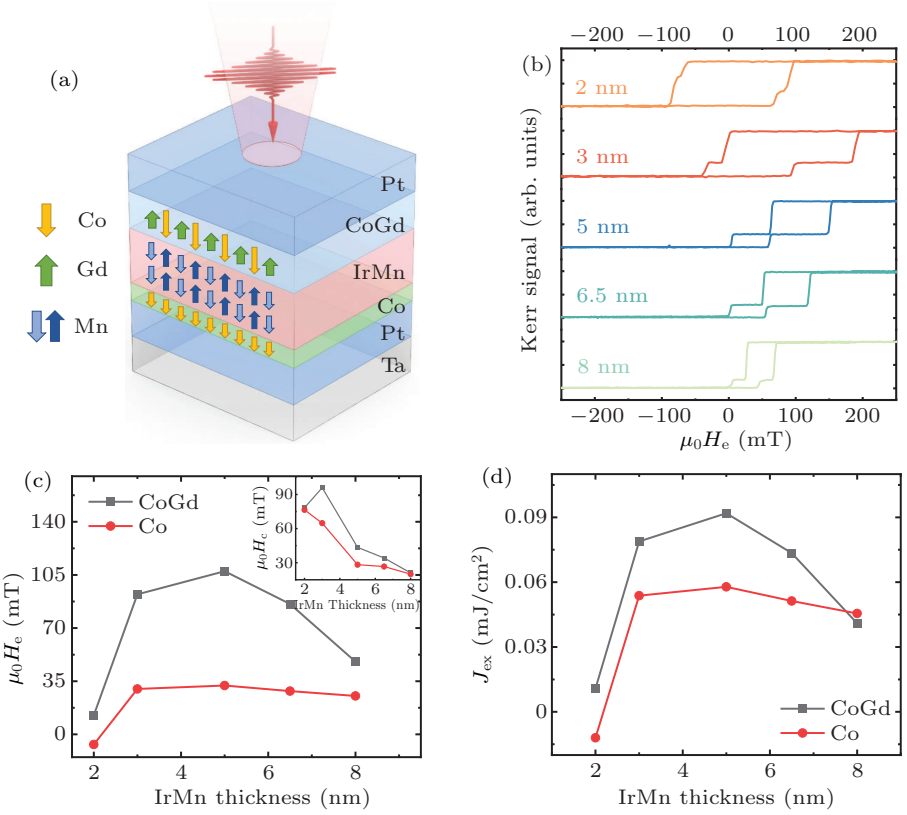


Fig. 1. The Co/IrMn/CoGd trilayers magnetic properties characterization. (a) Film stacks structure of Co/IrMn/CoGd perpendicular exchange bias trilayers system. (b) The hysteresis loops at various IrMn thicknesses (t_{IrMn} from 2 nm to 8 nm). Clear stepped hysteresis loops can be obtained at t_{IrMn} from 2 nm to 8 nm. (c) The exchange bias field $\mu_0 H_e$ and coercivity $\mu_0 H_c$ (inset) of CoGd and Co interface as a function of IrMn thickness. (d) The effective exchange coupling constant J_{ex} of both interfaces given by $J_{ex} = \mu_0 H_e M_s t$ as a function of the IrMn thickness (t_{IrMn}).

The effect of the IrMn layer thickness on the exchange bias field in bilayer systems has been extensively studied.[5] Generally, in an IrMn exchange-biased bilayer system, the exchange bias field rapidly increases above the critical thickness (t_c), reaches a maximum (t_{max}), then saturates. This behavior is attributed to the interplay between the interfacial ex-

change bias and the AFM anisotropy of the IrMn layer. As the thickness of the IrMn layer increases, the interfacial exchange bias becomes less dominant, and the AFM anisotropy of the IrMn layer becomes the primary contributor to the exchange bias field.[5] Consequently, no additional AFM anisotropy is available to support the interfacial exchange bias, leading to the saturation of the exchange bias field beyond a certain thickness.[5] However, in the FM/IrMn/FM trilayers, the additional interlayer effect of the two FM layers must be considered. When IrMn layer thickness $t_{\mathrm{IrMn}} < t_{\mathrm{c}}$, the short-range interaction of the two interfaces is usually induced by RKKY interlayer coupling[23] or orange peel effect[24] and the long-range interaction ($t_{\mathrm{IrMn}} > t_{\mathrm{max}}$) shows the exchange spring behavior.[25] When $t_{\mathrm{c}} < t_{\mathrm{IrMn}} < t_{\mathrm{max}}$, there will be an interplay between the interlayer coupling and the AFM anisotropy of the IrMn layer, which usually induces exchange bias enhancement and propagation phenomenon of the two interfaces.[10–12] In polycrystalline IrMn structures, the size of the grains must be taken into account as a crucial factor in the propagation of exchange bias.[23,24] The hysteresis loops of Co (1)/IrMn (t_{IrMn})/$Co_{77}Gd_{23}$ (4) trilayers with $t_{\mathrm{IrMn}} = 3$–8 nm are shown in Figs. 2(a)–2(d). The major loops (black) reflect the full switching of the entire structure. The minor loops (red) only reflect the reversal of the CoGd layer without Co layer reversal. We can note that the overlapping of the major and minor loops differs in various IrMn layer thicknesses. For the thinner 3 nm and 5 nm IrMn layers Figs. 2(a) and 2(b), without Co layer switching, the right branch of the CoGd loop shifts leftward. However, for the thicker 6.5 nm and 8 nm IrMn layers Figs. 2(c) and 2(d), the CoGd subloops almost overlap with the major and minor loops. When $t_{\mathrm{IrMn}} = 6.5$ nm and 8 nm, the exchange bias generates by the AFM grains of each side and keeps independent during the magnetization reversal. When $t_{\mathrm{IrMn}} < 5$ nm, after the full switching of the trilayers, the nonrecoverable reversal of the AFM spins occurs in the Co/IrMn interface propagating through interlayer coupling across the AFM volume orders and acting on the IrMn/CoGd interface.[11] In addition, the interlayer coupling can be seen as an energy barrier and partially unlock the exchange coupling of CoGd after Co fully switched.[11] With the strong interlayer coupling of the two interfaces, the AFM volume orders can be well characterized by the interfacial exchange bias and help us further explore the interfacial and volume AFM orders rearrangement under the femtosecond laser-induced ultrafast dynamics.

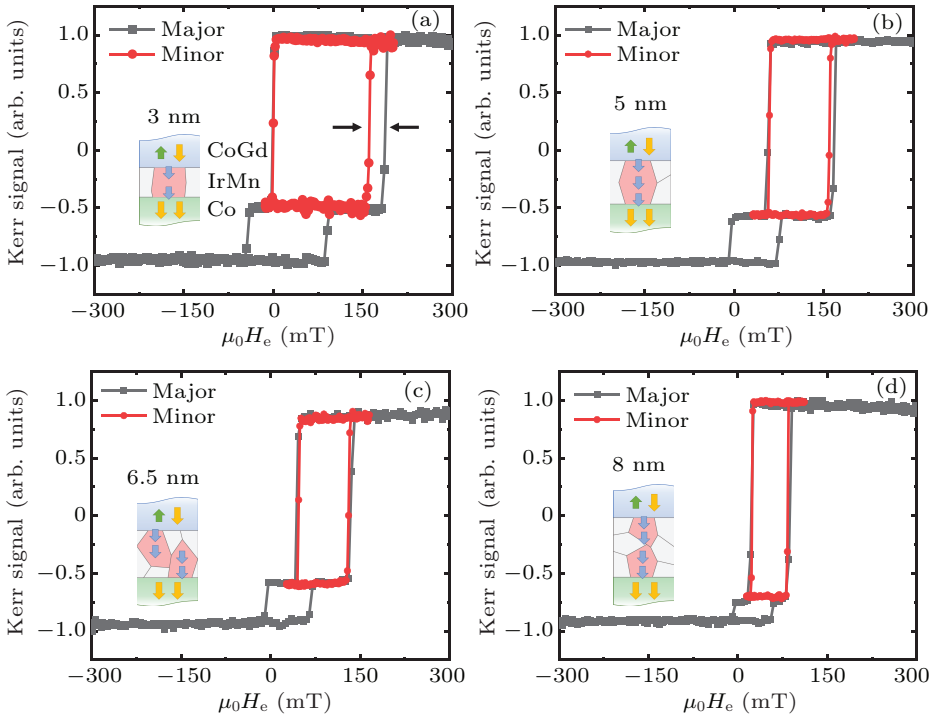


Fig. 2. The interlayer coupling of the Co/IrMn and IrMn/CoGd interfaces. (a)–(d) Major (black) and minor (red) loops of Co (1)/IrMn (t_{IrMn})/$Co_{77}Gd_{23}$ (4) trilayers with $t_{\mathrm{IrMn}} = 3$ nm, 5 nm, 6.5 nm and 8 nm. When $t_{\mathrm{IrMn}} = 3$ nm and 5 nm, the right branch of the minor loop shows a clear leftward shift. When $t_{\mathrm{IrMn}} = 6.5$ nm and 8 nm, the major and minor loops overlap with each other.

3. Laser-induced ultrafast antiferromagnet rearrangement

Single-shot laser-induced exchange bias switching at IrMn/CoGd interface was performed for various laser fluences with IrMn thickness t_{IrMn} ranging from 3 nm to 8 nm in Figs. 3(a)–3(d). The experiments were carried out by a Ti:sapphire femtosecond laser with a 5-kHz repetition rate and a wavelength of 800 nm (1.55 eV). The pulse duration is 40 fs and the full width at half maximum (FWHM) of the beam diameter is ~ 50 μm. The exchange bias field of both interfaces was obtained at the center of the excitation region, which was measured using a MOKE microscope. Due to the laser-

induced heating, the temperature of the trilayer system exceeded the Néel temperature of the IrMn layer. Time-resolved experiments have shown that the exchange bias of IrMn-based systems quenches at 0.7±0.5 ps.[26] In our previous work, we indicated that the IrMn/CoGd bilayer system exhibits AO-HIS with a switching timescale of ∼ 5 ps, and demonstrated that the single shot exchange bias switching arises from the coherent switching process of the coupled IrMn grains, induced by ultrafast CoGd switching.[21] Through the time-resolved measurement, we have shown that the interfacial exchange bias switching occurs within 100 ps.[21] In the meantime, the exchange bias of the Co/IrMn interface is only affected by laser heating and the interacted AFM spin configuration itself.[27] In Fig. 3, we can note that the maximum amplitude of the exchange bias switching at the IrMn/CoGd interface decreases with the increased IrMn thickness. Compared to the initial exchange bias after annealing, 37%–19% of the switched exchange bias varies from 3 nm to 8 nm IrMn thickness. However, the exchange bias of the Co/IrMn interface reduces close to zero at $t_{\mathrm{IrMn}} = 3$ nm and remains positive at $t_{\mathrm{IrMn}} = 5$ nm, 6.5 nm and 8 nm, but is much less pronounced. We can conclude that: 1) The exchange bias reduction of two interfaces indicates that under such an ultrafast laser excitation process, the recovery of the AFM volume orders is not fully deterministic and thus does not allow the interfacial AFM spins to rearrange completely. 2) The amplitude of exchange bias switching in IrMn/CoGd decreases as the thickness of IrMn increases. This effect is attributed to the attenuated interfacial coupling, as depicted in Fig. 1(d). 3) The ultrafast demagnetization and antiparallel final state cause a twist in the AFM volume orders, which leads to zero exchange bias at the Co/IrMn interface.

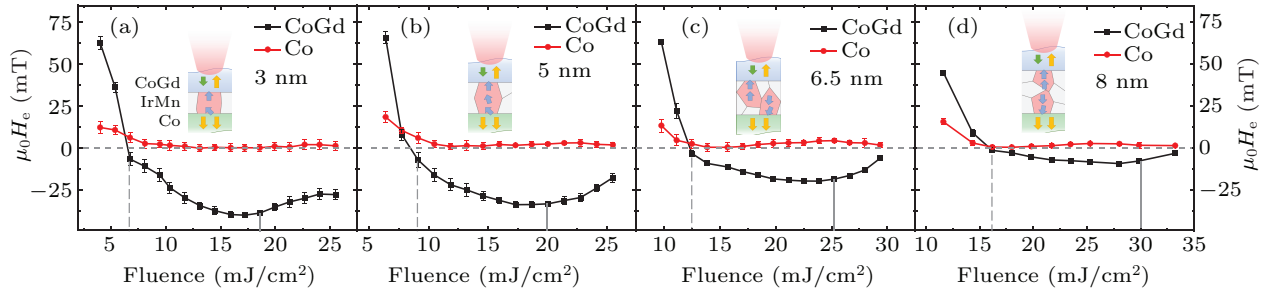


Fig. 3. Single-shot exchange bias switching in Co/IrMn/CoGd trilayers. (a)–(d) Exchange bias field of CoGd and Co interface in 3 nm, 5 nm, 6.5 nm and 8 nm IrMn samples after shining by a single linearly polarized laser pulse with a pulse duration of 40 fs and various fluences. The vertical dash line indicates the threshold fluence of CoGd switching and the solid line indicates the demagnetization fluence that CoGd begins to demagnetize.

From the fluence-dependent exchange bias switching at various IrMn thicknesses, we can only observe the ultrafast AFM spins rearrangement at the IrMn/CoGd interface, and the behavior of AFM volume orders is still unclear. Therefore, we focused on the Co (1)/IrMn (3)/CoGd (4) sample and utilized the exchange bias variation of the two interfaces. The trilayer system with $t_{\mathrm{IrMn}} = 3$ nm suggests a strong interlayer interaction in the IrMn volume order. The recovery of exchange bias after laser excitation depends on AFM spins rotation at both interfaces, as well as the competition or propagation during the rearrangement of AFM volume orders in the antiparallel (AP) or parallel (P) configuration of the two interfaces. Firstly, we start from the P initial state, as shown in Fig. 4(a). After laser excitation, the exchange bias of the IrMn/CoGd interface switches to negative (CoGd-*a*), Co layer remagnetization to initial but the exchange bias reduces to zero (Co-*a*) over the fluence of CoGd switching threshold (vertical dash line), as shown in Fig. 4(c). In the other case, we use the external field to reverse the Co layer to AP configuration but with initial positive exchange bias (Fig. 4(b)). After the laser shines at zero fields, the exchange bias of both interfaces switches to negative after CoGd begins switching (CoGd-*b* and Co-*b* in Fig. 4(c)). From the fluence dependence of the CoGd interfacial exchange bias with different Co states, we can note that, in the all-optical switching window of CoGd (between the solid and dash lines), the AFM spins rearrangement of the IrMn/CoGd interface is not affected by the Co/IrMn interface state, which represents almost the same AFM spin configuration at the IrMn/CoGd interface. But the P final state after laser excitation allows the AFM layer to further reorder without forming a twist domain wall and propagates to the Co/IrMn interface.[11,12] Over 17 mJ/cm^2, CoGd demagnetizes and gradually becomes a multidomain state. The exchange bias reduces toward zero, and the AFM spin orders at the IrMn/CoGd interface can not be well defined. However, with the higher temperature and longer time heating, the negative exchange bias of the Co/IrMn interface (Co-*b*) can lead to the additional pinning of the AFM layer compared to the zero exchange bias situation (Co-*a*) and result in the exchange bias field of IrMn/CoGd negative shift (CoGd-*b*) compared to the AP final state (CoGd-*a*). Accordingly, it is observed that the competition and propagation of exchange bias can be discerned over a broad range of laser fluence. Within the switching window of CoGd, the reorientation of AFM spins at the IrMn/CoGd interface can be efficiently achieved through a single laser pulse, which further influences the AFM volume orders. When the laser fluence exceeds the switching window and CoGd loses its dominance of the interfacial AFM spins,

the exchange bias of the IrMn/CoGd interface is found to be sensitive to different AFM order configurations owing to the interlayer interaction.

Furthermore, we investigate the exchange bias repeated switching by multi-pulses excitation. We increase the number of laser pulses with a fluence of 16 mJ/cm^2 to shine from the P (Fig. 5(a)) and AP (Fig. 5(b)) initial state, respectively. The AP initial state is obtained by reversing the Co layer with an external field and then removing the field when shining the laser. The related continuous switching results are shown in Figs. 5(c) and 5(d), a repeatable and stable exchange bias switching can be found at the IrMn/CoGd interface in the range of ±40 mT in both situations. On the contrary, the exchange bias of the Co/IrMn interface shows a constant value ($\sim$ 0 mT and −8 mT) after the first pulse. Then we use higher fluence with 21 mJ/cm^2 over the CoGd switching window, as shown in Figs. 5(e) and 5(f). At the odd number of laser pulses, the CoGd layer begins to demagnetize and the amplitude of the switched exchange bias of the IrMn/CoGd interface starts to decrease according to Fig. 4(c). However, a significant difference can be noted in the back-switched exchange bias amplitude at the even number of pulses on different Co states (Figs. 5(e) and 5(f)). The demagnetization of CoGd at high fluence will lose dominance on AFM orders, and the effective exchange bias of Co/IrMn can propagate to the IrMn/CoGd interface.[11,12] As shown in Fig. 5(f), the negative exchange bias of the Co/IrMn interface effectively prevents the back-switched exchange bias of the IrMn/CoGd interface. Therefore, after the first laser excitation, the antiferromagnetic (AFM) orders may transit into a metastable state depending on the initial configuration of the two interfaces. The independent behavior of the interfaces upon subsequent laser pulse excitation provides further evidence that the exchange bias switching of the IrMn/CoGd interface is primarily driven by the rearrangement of interfacial AFM spins. Moreover, the AO-HIS of the coupled CoGd layer can be utilized as an ultrafast reset method for the AFM.

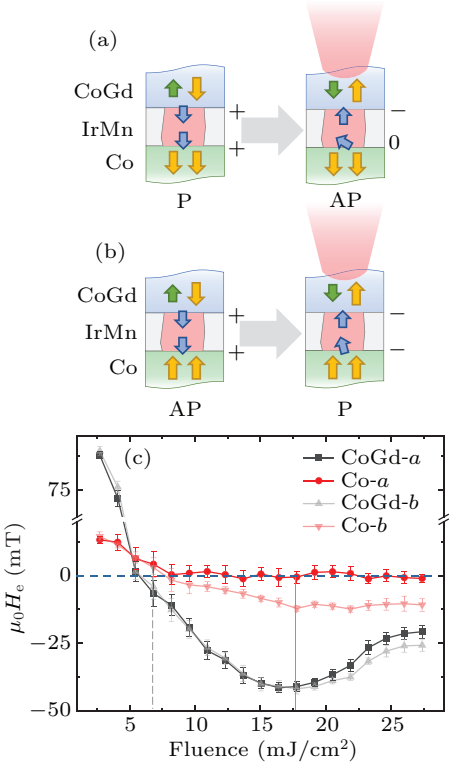


Fig. 4. The single-shot exchange bias switching with different Co states at t_{IrMn} = 3 nm. (a) Switching to the final state (AP) from the initial after-annealing state (P). (b) Shining the laser on the AP initial state and switching to P final state after reversing Co layer by an external field. (c) Evolution of $\mu_0 H_e$ of different CoGd and Co initial states after excitation by one single laser pulse as a function of the laser fluence. Curves CoGd-*a* and Co-*a* represent the evolution of $\mu_0 H_e$ from P initial state. Curves CoGd-*b* and Co-*b* represent the evolution of $\mu_0 H_e$ from AP initial state. The vertical dash line indicates the threshold fluence of CoGd switching and the solid line indicates the demagnetization fluence that CoGd begins to gradually become a multidomain state.

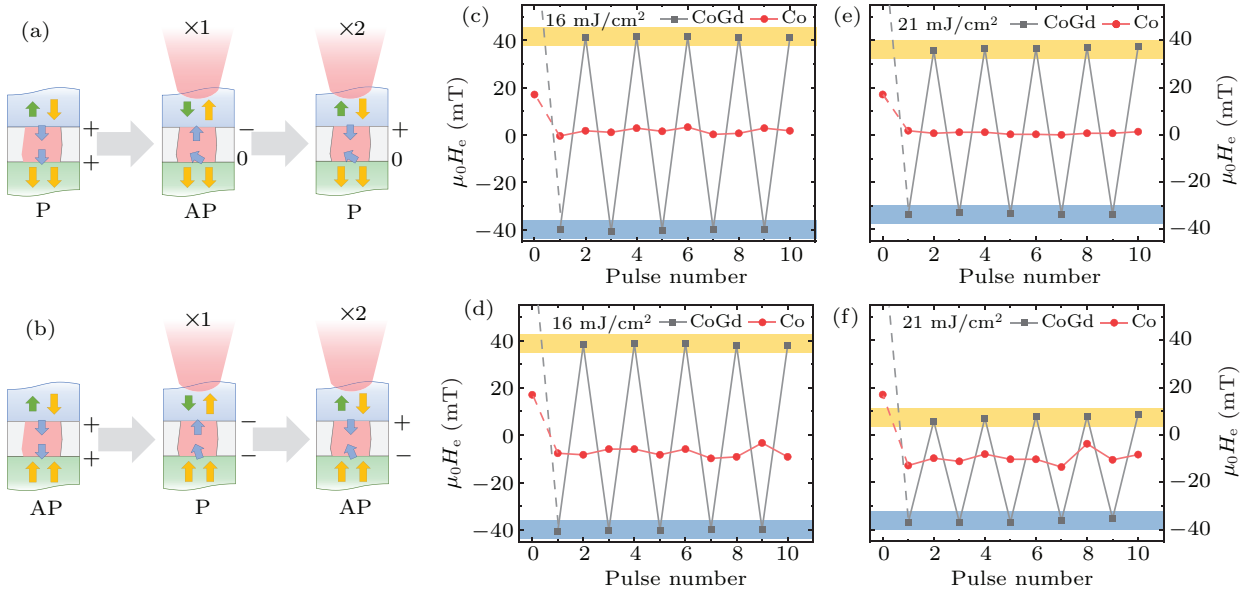


Fig. 5. Exchange bias switching with the number of pulses at different Co states. (a) The laser excitation from the P initial state with a laser fluence of (c) 16 mJ/cm^2 and (e) 21 mJ/cm^2. (b) The laser excitation from AP initial state with a laser fluence of (d) 16 mJ/cm^2 and (f) 21 mJ/cm^2.

4. Conclusion and perspectives

In this work, we investigated dual perpendicular exchange bias systems in Co/IrMn/CoGd trilayers using both static field switching and ultrafast all-optical manipulation. Our results demonstrate the IrMn thickness-dependent interlayer coupling between the two exchange bias interfaces and reveal that the exchange bias at the IrMn/CoGd interface can be effectively controlled with a single femtosecond laser pulse. This manipulation is attributed to the ultrafast rearrangement of AFM spins at the interface, which also has a significant impact on the AFM volume orders. Furthermore, our observations of the competition between the Co/IrMn and IrMn/CoGd exchange-biased interfaces under ultrafast dynamics highlight the effectiveness of the AO-HIS in enhancing the efficiency of the coupled AFM manipulation. These findings provide new insights into exchange bias phenomena and have implications for the development of ultrafast, field-free, and energy-efficient antiferromagnet manipulation techniques.

Acknowledgements

The authors gratefully acknowledge the National Key Research and Development Program of China (Grant No. 2022YFB4400200), the National Natural Science Foundation of China (Grant Nos. 12104030, 12104031, and 61627813), the Program of Introducing Talents of Discipline to Universities (Grant No. B16001), the Beijing Municipal Science and Technology Project (Grant No. Z201100004220002), China Postdoctoral Science Foundation (Grant No. 2022M710320), and China Scholarship Council. This work is also supported by the ANR-15-CE24-0009 UMAMI and the ANR-20-CE09-0013, by the Institute Carnot ICEEL for the project "Optic-switch" and Matelas, by the Région Grand Est, by the Metropole Grand Nancy, by the impact project LUE-N4S, part of the French PIA project "Lorraine Université d'Excellence," reference ANR-15-IDEX-04-LUE, and by the "FEDERFSE Lorraine et Massif Vosges 2014-2020," a European Union Program.

References

[1] Jungwirth T, Marti X, Wadley P and Wunderlich J 2016 *Nat. Nanotechnol.* **11** 231
[2] Xiong D, Jiang Y, Shi K, Du A, Yao Y, Guo Z, Zhu D, Cao K, Peng S, Cai W, Zhu D and Zhao W 2022 *Fundamental Research* **2** 522
[3] Meiklejohn W H and Bean C P 1957 *Phys. Rev.* **105** 904
[4] Ohldag H, Scholl A, Nolting F, Arenholz E, Maat S, Young A T, Carey M and Stöhr J 2003 *Phys. Rev. Lett.* **91** 017203
[5] Ali M, Marrows C H, Al-Jawad M, Hickey B J, Misra A, Nowak U and Usadel K D 2003 *Phys. Rev. B* **68** 214420
[6] Xu X Y, Wang M H and Hu J G 2008 *Chin. Phys. B* **17** 1443
[7] Qi X J, Yang N N, Duan X X and Li X Z 2021 *Chin. Phys. B* **30** 107501
[8] Chen Y T 2008 *Nanoscale Research Letters* **4** 90
[9] Morales R, Li Z P, Olamit J, Liu K, Alameda J M and Schuller I K 2009 *Phys. Rev. Lett.* **102** 097201
[10] Xu Y, Ma Q, Cai J W and Sun L 2011 *Phys. Rev. B* **84** 054453
[11] Zhan X Z, Li G, Cai J W, Zhu T, Cooper J F K, Kinane C J and Langridge S 2019 *Scientific Reports* **9** 6708
[12] Nam D N H, Chen W, West K G, Kirkwood D M, Lu J and Wolf S A 2008 *Appl. Phys. Lett.* **93** 152504
[13] Freitas P P, Ferreira R and Cardoso S 2016 *Proc. IEEE* **104** 1894
[14] Guo Z, Yin J, Bai Y, Zhu D, Shi K, Wang G, Cao K and Zhao W 2021 *Proc. IEEE* **109** 1398
[15] Sharma A, Hoffmann M A, Matthes P, Busse S, Selyshchev O, Mack P, Exner H, Horn A, Schulz S E, Zahn D R T and Salvan G 2019 *J. Mag. Magn. Mater.* **489** 165390
[16] Mangin S, Gottwald M, Lambert C H, Steil D, Uhlíř V, Pang L, Hehn M, Alebrand S, Cinchetti M, Malinowski G, Fainman Y, Aeschlimann M and Fullerton E E 2014 *Nat. Mater.* **13** 286
[17] Lambert C H, Mangin S, Varaprasad B S D Ch S, Takahashi Y K, Hehn M, Cinchetti M, Malinowski G, Hono K, Fainman Y, Aeschlimann M and Fullerton E E 2014 *Science* **345** 1337
[18] Wang L, Cheng H, Li P, van Hees Y L W, Liu Y, Cao K, Lavrijsen R, Lin X, Koopmans B and Zhao W 2022 *Proc. Natl. Acad. Sci. USA* **119** 2211953
[19] Vallobra P, Fache T, Xu Y, Zhang L, Malinowski G, Hehn M, Rojas-Sánchez J C, Fullerton E E and Mangin S 2017 *Phys. Rev. B* **96** 144403
[20] Radu I, Vahaplar K, Stamm C, Kachel T, Pontius N, Dürr H A, Ostler T A, Barker J, Evans R F L, Chantrell R W, Tsukamoto A, Itoh A, Kirilyuk A, Rasing Th and Kimel A V 2011 *Nature* **472** 205
[21] Guo Z, Wang J, Malinowski G, Zhang B, Zhang W, Wang H, Liu C, Peng Y, Vallobra P, Xu Y, Jenkins S, Chantrell R W, Evans R F L, Mangin S, Zhao W and Hehn M 2023 arXiv:2302.04510 [cond-mat]
[22] Malinowski G, Hehn M and Panissod P 2006 *J. Phys.: Condens. Matter* **18** 3385
[23] Moritz J, Vinai G and Dieny B 2012 *IEEE Magnetics Letters* **3** 4000204
[24] Moritz J, Bacher P, Auffret S and Dieny B 2011 *J. Magn. Magn. Mater.* **323** 2391
[25] Castro I L, Nascimento V P, Passamani E C, Takeuchi A Y, Larica C, Tafur M and Pelegrini F 2013 *J. Appl. Phys.* **113** 203903
[26] Dalla Longa F, Kohlhepp J T, de Jonge W J M and Koopmans B 2010 *Phys. Rev. B* **81** 094435
[27] Kumberg I, Golias E, Pontius N, Hosseinifar R, Frischmuth K, Gelen I, Shinwari T, Thakur S, Schüßler-Langeheine C, Oppeneer P M and Kuch W 2020 *Phys. Rev. B* **102** 214418